THE PHOTOGRAMMETRIC RECORD

*The Photogrammetric Record* (2021)
DOI: 10.1111/phor.12382

# AIRBORNE LIDAR PLANAR ROOF POINT EXTRACTION USING LEAST-SQUARES FITTING SUPERVISED BY A POSTERIORI VARIANCE ESTIMATION

Shih-Hong Chio* (chio0119@gmail.com)
Li-Cheng Chan (jy64973@gmail.com)
*National Chengchi University, Taipei, Taiwan*

*Abstract*

*The least-squares fitting method can be used for planar roof point extraction from airborne lidar points; however, it cannot avoid the impact of non-planar roof points (blunders) due to lack of robustness. Therefore, this study has developed a least-squares plane fitting based on a posteriori variance estimation, as proposed by Li in 1983, to reduce the weights of non-planar roof points. Additionally, least absolute deviation (LAD) was integrated into the first step of this improved Li method, to increase blunder detection. For simulated data, the proposed approach increased the blunder detection rate by up to 6% compared to the original Li method. Test results with real data showed that the proposed approach demonstrated robustness, applicability and effectiveness.*

Keywords: a posteriori variance estimation, blunder detection, LAD, least-squares fitting, lidar, selected weights

## Introduction

An airborne lidar system emits laser pulses to quickly capture high-resolution geospatial data such as digital surface models. The system is composed of a laser scanner combined with both a Global Navigation Satellite System (GNSS) and an inertial navigation system (INS), mounted on an aerial platform. Through the instrumental operation and process, the system creates accurate three-dimensional points (point clouds). Airborne lidar point clouds consist of large discrete 3D datasets. However, the geometric features are only implicit, so it is necessary to select a suitable method to extract geometric features from the point clouds for further processing. For 3D building models, roof points or planes in the airborne lidar data should be extracted first. Most of the existing methods, dating back to the turn of the century, transform the distributed lidar data into grid data through interpolation procedures and then apply image processing techniques to detect and extract these features (Maas and Vosselman, 1999; Geibel and Stilla, 2000). Thus, some important spatial information, especially that related to heighting accuracy, might be lost (Axelsson, 2000). For this reason, a number of algorithms that use the original airborne lidar data have been developed (Ackermann, 1999; Haala and Brenner, 1999; Priestnall et al., 2000; Vosselman and Dijkman, 2001; Gorte, 2002; Roggero, 2002; Schuster, 2004).

For example, Vosselman and Dijkman (2001) used the well-known Hough transform for the extraction of planar faces from irregularly distributed point clouds. If a laser dataset contains points in a planar surface, the planes of these points in the parameter space will intersect at the position corresponding to the slopes and distance of the planar surface. For the detection of this intersection point, the standard procedure of sampling the parameter space and searching for the bin with the highest number of planes can be used (Ballard and Brown, 1982). Roggero (2002) combined region growing techniques and principal component analysis (PCA) for roof extraction, in which PCA was used to define the aggregation criteria and to describe the geometrical properties of the objects. The result was obtained by working on raw data, so they were able to take advantage of the full resolution potential of laser scanning. Gorte (2002) used the original (triangulated) laser points to iteratively merge triangular irregular networks (TINs) and transform small segments into larger segments. The algorithm was regulated by a single parameter that controlled the maximum dissimilarity for adjacent segments such that merging them was still allowed. Schuster (2004) presented an investigation on the use of tensor voting for categorising lidar data into outliers, line elements (such as high-voltage power lines), surface patches (roofs) and volumetric elements (vegetation), which was based on segmentation of lidar data using a tensor voting framework. Tensor voting is a methodology for extracting salient features including surfaces, edges and corners inferred from tensor fields generated by the voting procedure among the point cloud. Wang and Tseng (2004) presented an octree-structure-based split-and-merge segmentation algorithm for organising airborne lidar point-cloud data into clusters of 3D planes. Recently, machine learning approaches based on lidar data for building extraction and roof shape classification have been used, and deep learning approaches have been shown to perform well for building detection. However, in most of these cases, their planimetric accuracies were low, and individual roof plane extraction was not considered (Dey et al., 2020).

Although the use of the original airborne lidar data can maintain the original accuracies, some difficulties still exist for planar roof point extraction from airborne lidar data. The challenging tasks are how to exclude the irrelevant points and how to extract planar roof points reliably and automatically. In order to extract appropriate planar roof points, noise interference must be excluded. Noise can be understood as non-planar points from other objects (for example, a chimney on the roof), which should be regarded as blunders while planar points are extracted. Thus, a common method is setting a threshold to eliminate a small number of blunders (Höhle, 2013). Chio (2005) presented an approach to automatically acquire 3D building roofs from airborne lidar data based on data snooping theory. Here, the best-fitting plane was obtained from the extracted TIN planes through the iterative merging of the fine TIN structures, constructed from the original airborne lidar data, by a forward selection algorithm. However, this approach is time-consuming. Forlani et al. (2003) and Khoshelham (2005) employed random sample consensus (RANSAC; Fischler and Bolles, 1981) to exclude non-roof points while extracting building planar roofs. If the observations containing blunders are thought of as a sample of large variance and of the same expectation, then it can lead to an iterative method with selected weights for positioning blunders (Li et al., 2015). Based on this concept, Chio (2008) developed an algorithm based on robust estimation theory to acquire planar roof lidar points and remove irrelevant non-planar roof points. In order to exclude the influence of these non-planar points, Chan and Chio (2017) developed an approach based on the selected weights supervised by a posteriori variance estimation presented by Li (Li, 1983; Li et al., 2015), called the Li method in this study, to reduce weights by the iteration method in order to extract the planar roof points accurately.

This study presents an extension of the approach presented by Chan and Chio (2017) in which the least absolute deviation (LAD) is combined with the Li method to exclude non-planar roof points. The latter are regarded as blunders and their weights are reduced by an iteration method in order to extract planar roof points accurately. Both simulated and actual airborne lidar data are used to verify the developed algorithm.

## Theory and Methodology

This section discusses the method for extracting planar roof lidar points and presents the relevant theories as well as the proposed approach. The evaluation method, based on simulated and real data, is also explained.

### *Least-squares Fitting*

In 3D Euclidean space, a roof plane can be formulated as equation (1):

$$a'x + b'y + c'z + d' = 0 \tag{1}$$

where *a', b', c'* and *d'* are the parameters of the plane, and *x*, *y*, *z* are the point coordinates. For planar roofs, including both horizontal (flat) and pitched (slanted) planar roofs, equation (1) can be simplified as equation (2):

$$z = ax + by + c \tag{2}$$

where *a*, *b* and *c* are the parameters of a plane and *x*, *y*, *z* are the point coordinates.

According to the rigorous least-squares adjustment, equation (2) can be rewritten as:

$$z_i + v_{z_i} = a(x_i + v_{x_i}) + b(y_i + v_{y_i}) + c$$

where $(v_{x_i}, v_{y_i}, v_{z_i})$ are the residuals of the $(x_i, y_i, z_i)$ coordinates at point *i*. This observation equation can be rearranged as:

$$a(x_i + v_{x_i}) + b(y_i + v_{y_i}) + c - (z_i + v_{z_i}) = 0. \tag{3}$$

Since equation (3) is non-linear, it should be linearised by the initial values ($a^0$, $b^0$, $c^0$) of unknowns and the rigorous least-squares adjustment of this plane should be solved by general least squares (Mikhail and Ackermann, 1976). The matrix form of general least squares is:

$$\mathbf{Ax} + \mathbf{Bv} + \mathbf{w} = 0 \tag{4}$$

where $\mathbf{A} = \begin{bmatrix} x_1 & y_1 & 1 \\ x_2 & y_2 & 1 \\ \vdots & \vdots & \vdots \\ x_4 & y_4 & 1 \end{bmatrix} \quad \mathbf{x} = \begin{bmatrix} da \\ db \\ dc \end{bmatrix}$

$$\mathbf{B} = \begin{bmatrix} a^0 & b^0 & -1 & 0 & 0 & 0 & \cdots & \cdots & \cdots & \cdots \\ 0 & 0 & 0 & a^0 & b^0 & -1 & 0 & \cdots & \cdots & \cdots \\ \vdots & \vdots & \vdots & \vdots & \vdots & \vdots & \vdots & \vdots & \vdots & \vdots \\ 0 & 0 & 0 & 0 & 0 & 0 & \cdots & a^0 & b^0 & -1 \end{bmatrix}$$

$$\mathbf{v} = \left[v_{x_1}\, v_{y_1}\, v_{z_1}\, v_{x_2}\, v_{y_2}\, v_{z_2} \cdots\cdots v_{x_n}\, v_{y_n}\, v_{z_n}\right]^{\mathrm{T}}$$

$$\mathbf{w} = \begin{bmatrix} -z_1 + x_1 a^0 + y_1 b^0 + c^0 \\ -z_2 + x_2 a^0 + y_2 b^0 + c^0 \\ \vdots \\ -z_n + x_n a^0 + y_n b^0 + c^0 \end{bmatrix}.$$

The unknown planar parameters can be determined by the following equation after an iterative solution:

$$\mathbf{x} = -\left[\mathbf{A}^{\mathrm{T}}\left(\mathbf{BP}^{-1}\mathbf{B}^{\mathrm{T}}\right)^{-1}\mathbf{A}\right]^{-1}\mathbf{A}^{\mathrm{T}}\left(\mathbf{BP}^{-1}\mathbf{B}^{\mathrm{T}}\right)^{-1}\mathbf{w} \tag{5}$$

where **P** is the weight matrix of the observations.

As rigorous least-squares adjustment, by general least squares, for the plane is too complicated and time-consuming, the residuals are only added to the corresponding $z$ coordinates. Therefore, equation (2) can be written as:

$$z_i + v_i = ax_i + by_i + c\,(i = 1,\ 2,\ \cdots,\ n).$$

where $v_i$ is the residual of the $z_i$ coordinate of point $i$. The above system of observation equations can be represented by the matrix notation, shown as equation (6):

$$\mathbf{Ax} = \mathbf{l} + \mathbf{v} \tag{6}$$

where $\mathbf{A} = \begin{bmatrix} x_1 & y_1 & 1 \\ x_2 & y_2 & 1 \\ \vdots & \vdots & \vdots \\ x_n & y_n & 1 \end{bmatrix}$ $\mathbf{x} = \begin{bmatrix} a \\ b \\ c \end{bmatrix}$ $\mathbf{l} = [z_1\, z_2 \cdots\cdots z_n]^{\mathrm{T}}$ $\mathbf{v} = [v_1\, v_2 \cdots\cdots v_n]^{\mathrm{T}}$.

By employing matrix algebra and the least-squares principle, the solution for equation (6) is:

$$\mathbf{x} = \left[\mathbf{A}^{\mathrm{T}}\mathbf{PA}\right]^{-1}\mathbf{A}^{\mathrm{T}}\mathbf{Pl}. \tag{7}$$

The a posteriori variance of unit weight is:

$$\hat{\sigma}_0^2 = \frac{v^T \mathrm{P} \mathrm{v}}{n-3} \tag{8}$$

where **P** is the weight matrix of the observations.

The difference between the two results (rigorous and simplified least-squares fitting for planar parameters) was compared and discussed in this study, and is described in a later section.

*Iterations Supervised by A Posteriori Variance Estimation*

While employing the least-squares fitting method for planar roof point extraction, it is unavoidable that points containing noise and non-planar roof points (which are regarded as blunders) should both be removed. Otherwise, the ordinary least-squares method will fail to solve the optimal estimated parameters because it cannot avoid the impact of blunders due to lack of robustness.

To solve this problem, these blunders should be detected and located. The data snooping method (Baarda, 1967) can be used to detect a single blunder by verifying the standardised residuals iteratively. However, there is a high possibility of numerous blunders existing in a least-squares problem. Robust estimation can be used to locate multiple blunders iteratively, with the goal of reducing the influence of blunders on the least-squares problem. There are numerous robust estimation categories. One category is least squares using iterations with the weights selected to reduce the weight of the observations with blunders and to exclude them. The key is to select the appropriate weight function. By using the proper weight function, observations with blunders will be detected and located and, thereby, excluded from the computation (Sisman, 2010).

The basic method of least squares using iterations with the selected weights is to first perform an initial least-squares adjustment, as the blunders are unknown. After that, the weights of the observations in each adjustment are recalculated according to the weight function defined by the residuals and relevant parameters. If the weight function is chosen properly and the blunders can be identified, the weights of the observations containing blunders will gradually decrease. When the iterations are suspended, the associated residuals will indicate the size of the blunder. Consequently, the result of the adjustment will not be impacted by blunders, and an accurate least-squares solution can be obtained (Li et al., 2015).

In this study, a least-squares fitting approach based on iterations with variable weights, which are supervised by a posteriori variance estimation, was proposed by Li (1983) and reiterated in Li et al. (2015). The authors have therefore called this the “Li method” in the current work. It was adopted to reduce the weights of non-planar roof points in order to accurately extract them. The basic concept of the Li method is to use a weight function calculated from the observation a posteriori variance, based on equation (9):

$$\hat{\sigma}_i^2 = \frac{\mathbf{v_i}^{\mathrm{T}} \mathbf{v_i}}{r_i} \tag{9}$$

where $i$ is the number of group $i$ (in this study $i$ is equal to 1); $r_i$ means the local redundancy of group $i$ and it is equal to $tr(\mathbf{Q_{vv}P})_i$ ($tr$ is the trace); $\mathbf{Q_{vv}}$ is the cofactor matrix of the residuals; and $\mathbf{P}$ is the weight matrix of the observations.

To verify if the $j$th observation contains a blunder, the statistical parameter $T_j$ is calculated using equation (10):

$$T_j = \frac{v_j^2}{\hat{\sigma}_0^2 r_j} \tag{10}$$

where $\hat{\sigma}_0$ is the a posteriori standard deviation and is equal to $\hat{\sigma}_i$ due to there being only one group of data; $v_j$ is the residual of the $j$th observation; and $r_j$ is equal to $q_{v_{jj}} p_j$.

The weight function is expressed as equation (11). During a given iteration $n$, the weight of the observations is 1 if they do not contain blunders; otherwise, they obtain a relatively small weight based on the statistical parameter $T_j$, where $T_j^{1/2}$ is calculated by equation (12). Based on the statistical test, the statistical parameter $T_j^{1/2}$ is used for testing, and threshold $K$ is set to discriminate possible blunders:

$$p_j^{(n+1)} = \begin{cases} 1 & \text{for } T_j^{1/2} \leq K \\ \dfrac{1}{T_j} & \text{for } T_j^{1/2} > K \end{cases} \tag{11}$$

$$T_j^{1/2} = \frac{v_j}{\hat{\sigma}_0\sqrt{r_j}} = \tau_j \tag{12}$$

where $T_j^{1/2}$ equals the statistics in Baarda's data snooping. It can be observed that the data snooping is equal to the first iteration of the current method. During the iterative process, to ensure that blunders are correctly positioned in rigorous conditions, $K$ is set as 1 during the first three iterations in the original Li method. After that, $K$ is set as 3.29 until the iterations are terminated due to the rate of change of the a posteriori variance being almost zero, that is:

$$\left| \frac{\hat{\sigma}_0^{(n+1)} - \hat{\sigma}_0^{(n)}}{\hat{\sigma}_0^{(n)}} \right| < 0.0001. \tag{13}$$

For a standard normal distribution, when $K$ is 1, for any group of measurements there will be approximately a 68.3% chance that any single observation will have an error between $\pm 1$; when $K$ is 3.29 there will be approximately a 99.9% chance of an error between $\pm 3.29$.

However, if the observations contain large blunders, the results of the first least-squares adjustment will be affected, even when the strict threshold ($K = 1$) for the statistical test is set, and it will possibly obtain bad parameter estimations that lead to the failure of the Li method. Therefore, the first step of the least-squares adjustment must still be performed using equal weights, because the number and locations of the blunders are uncertain. This can cause blunders to be assigned to other residuals and affect the determination of the observation weights in the next step of the least-squares adjustment. If the first step can determine the residuals that can reflect blunders more accurately, the corresponding observations can reduce the weights and increase the robustness.

*Least Absolute Deviations.* The LAD method is a robust estimation method. The theory of LAD, called the L1 norm, was developed by Boscovich (1757). The theory of LAD is based on a set of point data ($x_i$, $y_i$), $i = 1, 2, 3 \ldots n$, where $p_i$ is the weight of observation $y_i$. The object is to find the function $f(x_i)$ approximating $y_i$, where $f(x_i)$ can be either a linear or non-linear equation. The objective function, shown as equation (14), is used to minimise the sum of the weighted absolute values of the residuals $v_i$, that is, $|y_i - f(x_i)|$:

$$\varphi = \sum_{i=1}^{n} p_i |y_i - f(x_i)| = \sum_{i=1}^{n} p_i |v_i| = min. \tag{14}$$

The above function is difficult to calculate by differentiating due to the absolute value, and a direct solution is not possible except in special cases. A solution for the LAD method can be achieved by converting it to a linear programming problem and this consists of a constraint equation and an objective function, which must be positive. The mathematical model is expressed as:

$$
\begin{gathered}
\text{Minimise } \varphi = c_1x_1 + c_2x_2 + \cdots + c_nx_n \\
\text{subject to: } a_{11}x_1 + a_{11}x_2 + \cdots + a_{1n}x_n \le b_1 \\
a_{21}x_1 + a_{22}x_2 + \cdots + a_{2n}x_n \le b_2 \\
\vdots \\
a_{m1}x_1 + a_{m2}x_2 + \cdots + a_{mn}x_n \le b_m \\
x_1, x_2, \cdots x_n \ge 0
\end{gathered} \tag{15}
$$

where $x_1, x_2, \cdots x_n$ are decision variables; $c_1, c_2, \cdots c_n$ are the cost coefficients; $\varphi$ is the objective function; $a_{ij}$ is the constraint coefficient; and $b_i$ is a coefficient. The $i$th linear constraint condition is:

$$\sum_{j=1}^{n} a_{ij}x_j = b_i(i = 1, \cdots m,\ j = 1, \cdots n.).$$

The matrix form of equation (15) can be shown as equation (16):

$$
\begin{gathered}
\text{Minimise } \varphi = \mathbf{c}^{\mathbf{T}}\mathbf{x} \\
\text{subject to } \mathbf{Ax} = \mathbf{b} \\
x \ge 0.
\end{gathered} \tag{16}
$$

The decision variables should be positive, therefore $x_i$ is expressed by two non-negative real numbers, $x_i^+ x_i^-$, in equation (17) to determine the positive or negative decision variables:

$$
\begin{gathered}
x \in R; x_i^+ = \begin{cases} x_i \text{ if } x_i \ge 0 \\ 0 \ otherwise \end{cases}; x_i^- = \begin{cases} 0 \text{ if } x_i \ge 0 \\ -x_i \ otherwise \end{cases} \\
x_i^+, x_i^- \ge 0; x_i = x_i^+ - x_i^-; |x_i| = x_i^+ + x_i^-.
\end{gathered} \tag{17}
$$

For the property of positive decision variables, if $x_i$is positive, then $x_i^+$is 0; if $x_i$ is negative, then $x_i^+$ is 0.

Based on the concept in equation (17), an unknown vector $\mathbf{x}$ and residual vector $\mathbf{v}$ in the model of $\mathbf{Ax} = \mathbf{l} + \mathbf{v}$ can be expressed as the difference of two non-negative vectors. Furthermore, $|\mathbf{v}|$ can be expressed as the sum of two non-negative vectors, as shown in equation (18), and the constraint conditions in matrix form are $\mathbf{Ax} - \mathbf{v} = \mathbf{l}$.

$$\mathbf{x} = \mathbf{x}^{+} - \mathbf{x}^{-}\,;\, \mathbf{v} = \mathbf{v}^{+} - \mathbf{v}^{-}. \tag{18}$$

Vectors **x** and **v** in equation (18) are substituted into **Ax − v = l** to get:

$$[\mathbf{A} \quad -\mathbf{A} \quad -\mathbf{I} \quad \mathbf{I}] \begin{bmatrix} \mathbf{x}^{+} \\ \mathbf{x}^{-} \\ \mathbf{v}^{+} \\ \mathbf{v}^{-} \end{bmatrix} = \mathbf{l}. \tag{19}$$

Using $|\mathbf{v}| = \mathbf{v}^{+} - \mathbf{v}^{-}$ in equation (18), the objective function becomes equation (20):

$$\mathbf{c}^{\mathbf{T}}\mathbf{x} = [\mathbf{P}|\mathbf{v}|] = \mathbf{P}^{\mathbf{T}}|\mathbf{v}| = \mathbf{P}^{\mathbf{T}}|\mathbf{v}^{+} - \mathbf{v}^{-}| = min$$

$$\mathbf{c}^{\mathbf{T}}\mathbf{x} = \begin{bmatrix} 0 & 0 & \mathbf{P}^{\mathbf{T}} & \mathbf{P}^{\mathbf{T}} \end{bmatrix} \begin{bmatrix} \mathbf{x}^{+} \\ \mathbf{x}^{-} \\ \mathbf{v}^{+} \\ \mathbf{v}^{-} \end{bmatrix} = min. \tag{20}$$

The linear programming solution is determined by the simplex method (Dantzig, 1987; Williams, 2017). The following procedure is used to solve a linear programming problem in standard form:

(1) Write down the augmented matrix of the system of equations. This is called the initial simplex tableau.
(2) Locate the negative element in the last row (other than the last element) that is largest in magnitude. If two or more entries share this property, any one of these can be selected. If all such entries are non-negative, the tableau is in its final form.
(3) Divide each positive element in the column defined by this negative entry into the corresponding element of the last column.
(4) Select the divisor that yields the smallest quotient. This element is called a pivot element. If two or more elements share this property, any one of these can be selected as a pivot.
(5) Use row operations to create a one (1) in the pivot location and zeros (0) elsewhere in the pivot column.
(6) Repeat steps (2) to (5) until all such negative elements have been eliminated from the last row. The final matrix is called the final simplex tableau and leads to the optimal solution.

In this study, LAD was combined with the first step of the Li method, which the authors have called the improved Li method. The aim was to obtain better parameter estimations for LAD based on its robustness, as well as to provide a better basis for locating the blunders of observations for subsequent adjustments.

In this study, the difference between the original Li method and the improved Li method was investigated. After blunders were removed, the final results of the least-squares fitting were determined again with the same weight for all observations. Meanwhile, the standard deviation of unit weight was calculated.

### Evaluation

In this study, simulated airborne lidar points with rectangular horizontal planar roof data were used for testing. First, the difference between the ordinary least-squares and general least-squares fitting using simulated rectangular horizontal planar roof points with random errors was investigated. Then, the comparison among LAD, the Li method and the proposed improved Li method was presented using simulated rectangular planar roof points with different blunders. Finally, real data collected in Taiwan was used to test and verify the blunder detection ability of the proposed improved Li method. The evaluation was performed using the detectable blunder numbers and the rate of detectable blunders, and the coordinate comparison of the centroid calculated by the extracted rectangular planar roof points and the centroid calculated by the four roof corner coordinates as surveyed by a total station instrument. The coordinate comparison was performed in such a manner because the four roof corner coordinates could not be precisely measured by an airborne lidar scanning system; therefore, it would be much less reliable to simply use the root mean square error (RMSE) of the roof corner coordinate difference to evaluate the results. Meanwhile, the ISPRS Vaihingen data in Germany was used to evaluate the extraction results by a classification confusion matrix to reveal the recall, accuracy and precision.

## Results and Discussion

### Comparison between the Ordinary and General Least-squares Fitting

Fig. 1 shows a set of simulated points distributed evenly on a rectangular horizontal planar roof with a 10 m length and 5 m width. The point density was 1 pt/m$^2$ and there were a total of 66 points. A random error, generated with a 10 cm standard deviation, was added to each vertical and horizontal coordinate component randomly. The fitting results using ordinary and general least squares are tabulated as shown in Table I.

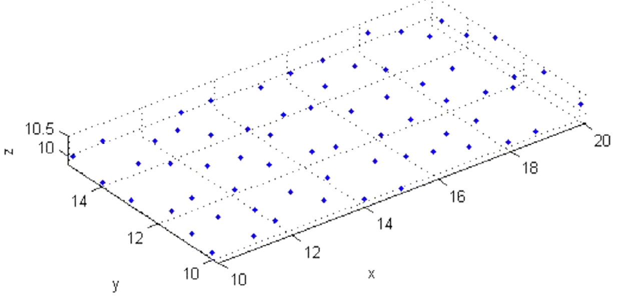


Fig. 1. Simulation data.

Table I. Fitting results using ordinary and general least squares.

| *Plane parameter* | *Ordinary least squares* | *General least squares* |
|---|---|---|
| *a* | 0.0016518969503**1920** | 0.0016518969503**1079** |
| *b* | 0.006653763718**78779** | 0.006653763718**65057** |
| *c* | 9.89161739668**293** | 9.89161739668**309** |

Differences shown in bold.

From Table I, the differences between two sets of fitting planar parameters $a$, $b$ and $c$ are extremely small. To realise the differences in the $z$ coordinate on the four simulated planar corners, the equation $z = ax + by + c$ was used to determine the $z$ values according to these two sets of planar parameters. The result showed there was no significant difference in the $z$ coordinate according to the height accuracy of the airborne lidar scanning system. Therefore, the ordinary least-squares fitting model could be used for subsequent tests.

### *Comparison between the Li Method, LAD and the Improved Li Method*

This study verified the ability of blunder detection for the Li method, LAD and the improved Li method for the extraction of planar points. The simulated data was the same as in the previous subsection: however, random errors were added only to the $z$ coordinates.

Generally, a random error size greater than three times the standard deviation can be considered as a blunder with a probability of 0.3%. Therefore, error sizes of four and five times the standard deviation (and even larger), meaning blunders with 0.4, 0.5, 1 and 2 m errors, were randomly added to the test data and used as simulated data for testing. A visual comparison of the blunder detection ability using the Li method and the improved Li method is presented in Fig. 2, in which the ordinates represent the number of detected blunders and the abscissas indicate the percentage of detected blunders.

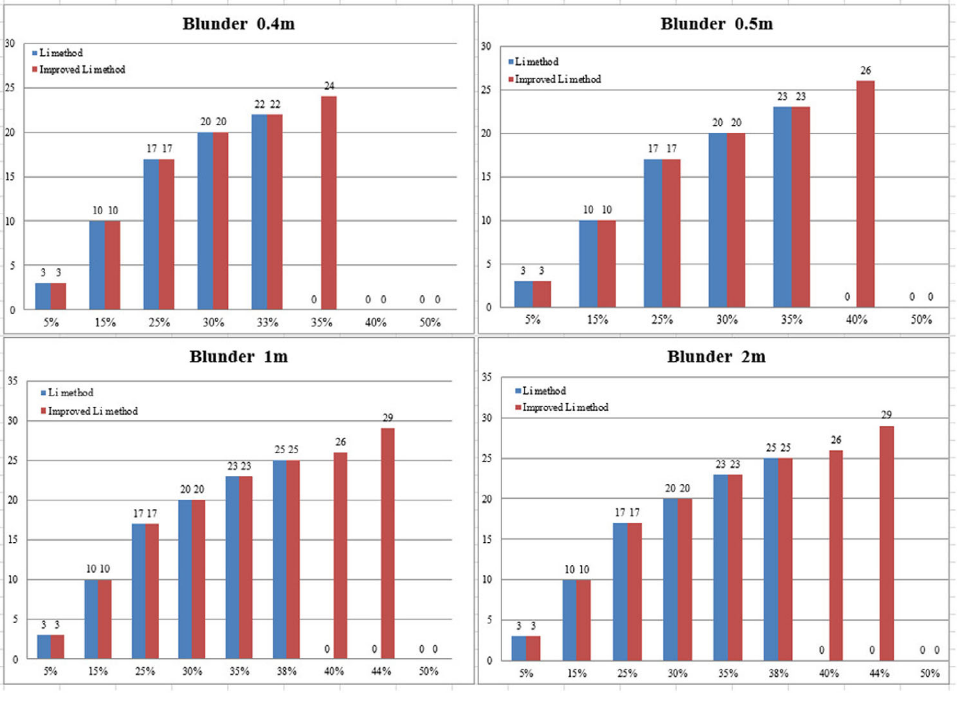


Fig. 2. Comparison of the blunder detection ability using the Li method (blue) and the improved Li method (red) for blunders of 0.4, 0.5, 1 and 2 m.

Table II. Detected and located blunders using the LAD method.

| *Percentage of blunders* | *No. of blunders* | *No. of blunders detected* | *Blunder size* | | | |
|---|---|---|---|---|---|---|
| | | | *0.4 m* | *0.5 m* | *1.0 m* | *2 m* |
| | | | *A posteriori standard deviation (m)* | | | |
| **5%** | **3** | **3** | **0.122** | **0.137** | **0.236** | **0.440** |
| 15% | 10 | 0 | 0.173 | 0.202 | 0.398 | 0.783 |
| 25% | 17 | 0 | 0.198 | 0.251 | 0.510 | 1.022 |
| 35% | 23 | 0 | 0.224 | 0.273 | 0.541 | 1.183 |
| 40% | 26 | 0 | 0.225 | 0.278 | 0.593 | 1.226 |
| 50% | 33 | 0 | 0.237 | 0.283 | 0.582 | 1.130 |

From the tests, the detected and located percentage of blunders using the improved Li method were about 35% and 40% when the blunder sizes were 0.4 and 0.5 m, respectively. The detected and located percentage of blunders were both 44% when the blunder sizes were 1 and 2 m, respectively. The improved Li method increased the rate of blunder detection by about 2% to 6% compared to the Li method. Table II shows the detected and located blunders using LAD. Table II indicates that LAD is a robust estimation method, and the LAD result could obtain the planar parameters and corresponding residuals of the observations. However, no reliable procedure can be used to verify if an observation contains a blunder. Therefore, the a posteriori standard deviation was determined to find the residuals with a blunder by verifying if the value was greater than three times the a posteriori standard deviation or not. From the tests, only 5% of blunders could be totally detected and located, no matter what blunder sizes were added.

### *Actual Taiwan Test Data*

From the simulated data tests, almost 44% of the blunders could be located in the observations with larger blunders (that is, 1 or 2 m blunders) under the proposed improved Li method. However, real data is more complicated, as the size and number of blunders are unknown. Therefore, this study used actual Taiwan data to test the improved Li method for the extraction of planar roof points. For the actual Taiwan data test, airborne lidar data covering Nangang Industrial Park in Nantou City, Taiwan was used. The point density was about 5.42 pt/m$^2$. Table III shows the orthoimages of six rectangular horizontal planar roofs superimposed with lidar points, their corresponding Google Street View images and their centroid coordinates calculated from the four corner roof point coordinates surveyed by a total station instrument.

The results are shown in Fig. 3 and Table IV. In Fig. 3, the red points represent non-planar roof points and the green points are the extracted roof points. As shown in Table IV, the coordinate differences are calculated by comparison of the centroid calculated by the extracted rectangular planar roof points and the centroid coordinates shown in Table III. From the results, it was deduced that the F16 and F201 datasets contained too many non-planar roof points to detect them. For the other four datasets, the corresponding non-planar roof points were detected. The non-planar roof point rates were 27%, 28%, 28% and 35% for the F10, F12, F45 and F124 datasets, respectively. The coordinate differences in the $E$, $N$, $H$ coordinate components were reasonable, and the fitting standard deviations were all between 2 and 8 cm; therefore, the proposed approach successfully extracted the roof points from these four datasets.

For the F16 and F201 datasets, as shown in Fig. 3, it could be possible that the rates of the non-roof points could still be too high to obtain better approximations of the planar

Table III. Six datasets of actual data used to test the improved Li method.

| *No.* | *Centroid coordinates (m)* | *Lidar points superimposed on orthimage* | *Google Street View images* |
|---|---|---|---|
| F10 | E: 215 105.467<br>N: 2 647 251.043<br>H: 213.878 |  |  |
| F12 | E: 215 209.703<br>N: 2 647 330.177<br>H: 201.856 |  |  |
| F16 | E: 215 057.989<br>N: 2 647 063.474<br>H: 224.974 |  |  |
| F45 | E: 214 890.067<br>N: 2 646 938.699<br>H: 244.152 | 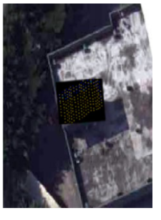 | 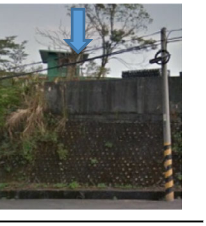 |
| F124 | E: 215 478.802<br>N: 2 647 021.457<br>H: 200.459 |  |  |
| F201 | E: 215 700.048<br>N: 2 646 795.469<br>H: 196.077 |  |  |

TABLE IV. Actual Taiwan data test using the improved Li method.

| | | | | | | |
|---|---|---|---|---|---|---|
| F10 | Centroid | E | 215 105.340 m | Coordinate difference | E | 0.127 m |
| | | N | 2 647 249.888 m | | N | 0.155 m |
| | | H | 213.856 m | | H | 0.023 m |
| | Fitting standard deviation | | 0.023 m | No. of detected non-roof points | | 733 |
| | Total points | | 2764 | Rate of detected non-roof points | | 27% |
| F12 | Centroid | E | 215 209.862 m | Coordinate difference | E | −0.159 m |
| | | N | 2 647 329.778 m | | N | 0.399 m |
| | | H | 201.937 m | | H | −0.08 m |
| | Fitting standard deviation | | 0.023 m | No. of detected non-roof points | | 52 |
| | Total points | | 184 | Rate of detected non-roof points | | 28% |
| **F16** | Centroid | E | 215 058.983 m | Coordinate difference | E | **−0.994 m** |
| | | N | 2 647 064.235 m | | N | **−0.761 m** |
| | | H | 223.870 m | | H | **1.104 m** |
| | Fitting standard deviation | | 1.184 m | No. of detected non-roof points | | **Undetected** |
| | Total points | | 299 | Rate of detected non-roof points | | **Unavailable** |
| F45 | Centroid | E | 214 890.379 m | Coordinate difference | E | −0.312 m |
| | | N | 2 646 938.571 m | | N | 0.128 m |
| | | H | 244.130 m | | H | 0.022 m |
| | Fitting standard deviation | | 0.018 m | No. of detected non-roof points | | 78 |
| | Total points | | 279 | Rate of detected non-roof points | | 28% |
| F124 | Centroid | E | 215 478.994 m | Coordinate difference | E | −0.192 m |
| | | N | 2 647 021.268 m | | N | 0.189 m |
| | | H | 200.398 m | | H | 0.061 m |
| | Fitting standard deviation | | 0.04 m | No. of detected non-roof points | | 61 |
| | Total points | | 173 | Rate of detected non-roof points | | 35% |
| **F201** | Centroid | E | 215 700.189 m | Coordinate difference | **E** | **−0.141 m** |
| | | N | 2 646 796.856 m | | **N** | **−1.387 m** |
| | | H | 192.335 m | | **H** | **3.742 m** |
| | Fitting standard deviation | | 4.081 m | No. of detected non-roof points | | **Undetected** |
| | Total points | | 678 | Rate of detected non-roof points | | **Unavailable** |

Problematic datasets shown in **bold**.

parameters using LAD in the first step of the improved Li method for excluding non-planar roof points and successfully extracting roof points. To verify this deduction, the lidar points around the centroid location (determined by the four roof corners surveyed by a total station) were extracted for calculation by LAD to obtain better planar parameter estimations. The results are shown in Fig. 4, in which the blue points represent the extracted points for calculation by LAD, the green points are the extracted points and the red points represent the detected non-planar roof points. The results (the coordinate differences, the number of detected non-planar roof points and the rate of detected non-planar roof points) for datasets F10, F12, F45 and F124 are the same as those shown in Table IV. Moreover, as shown in Table V, the roof points and non-planar roof points were successfully detected in dataset F16, as the fitting standard deviation is 2 cm and the coordinate differences were −0.468, 0.07 and 0.053 m in the E, N and H coordinate components, respectively. The rate of non-planar roof points was 36% in dataset F16. However, the improved proposed method (including LAD) still failed to detect the non-planar roof points in dataset F201.

From the previous test, if the datasets contained large non-planar roof points (that is, a large number of blunders), the LAD method would fail to acquire better planar parameter estimations for the improved Li method. Additionally, even if better planar parameters could

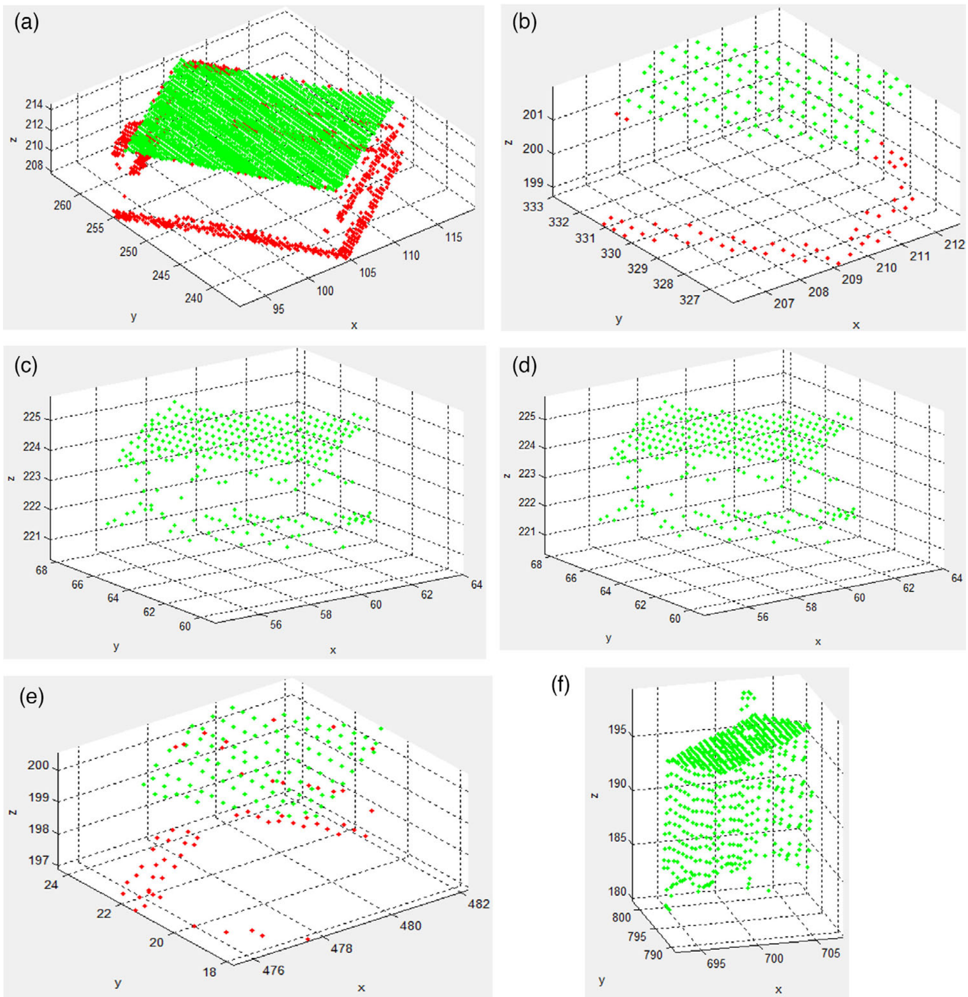


Fig. 3. The planar roof points (green) and non-planar roof points (red) extracted by the improved Li method. Note the lack of detected non-planar points in (c) and (f). The six datasets are also shown in Table III.

be determined, a large number of non-planar roof points could lead to the failure of the improved Li method. From Fig. 5 it is obvious that the F201 dataset contained numerous wall points. A visual verification indicated that the rate of non-planar roof points was over 50%. The results of the tests using both the simulated and real Taiwan datasets concluded that, with datasets where non-planar roof points constituted less than 35% of the total, the improved Li method will perform successfully. The improved Li method had the ability to detect more blunders than the original Li method according to the simulated data test results. However, how many blunders in a real dataset could be detected using the improved Li method still required verification. Therefore, the next test was used to discuss the blunder detection ability of the improved Li method.

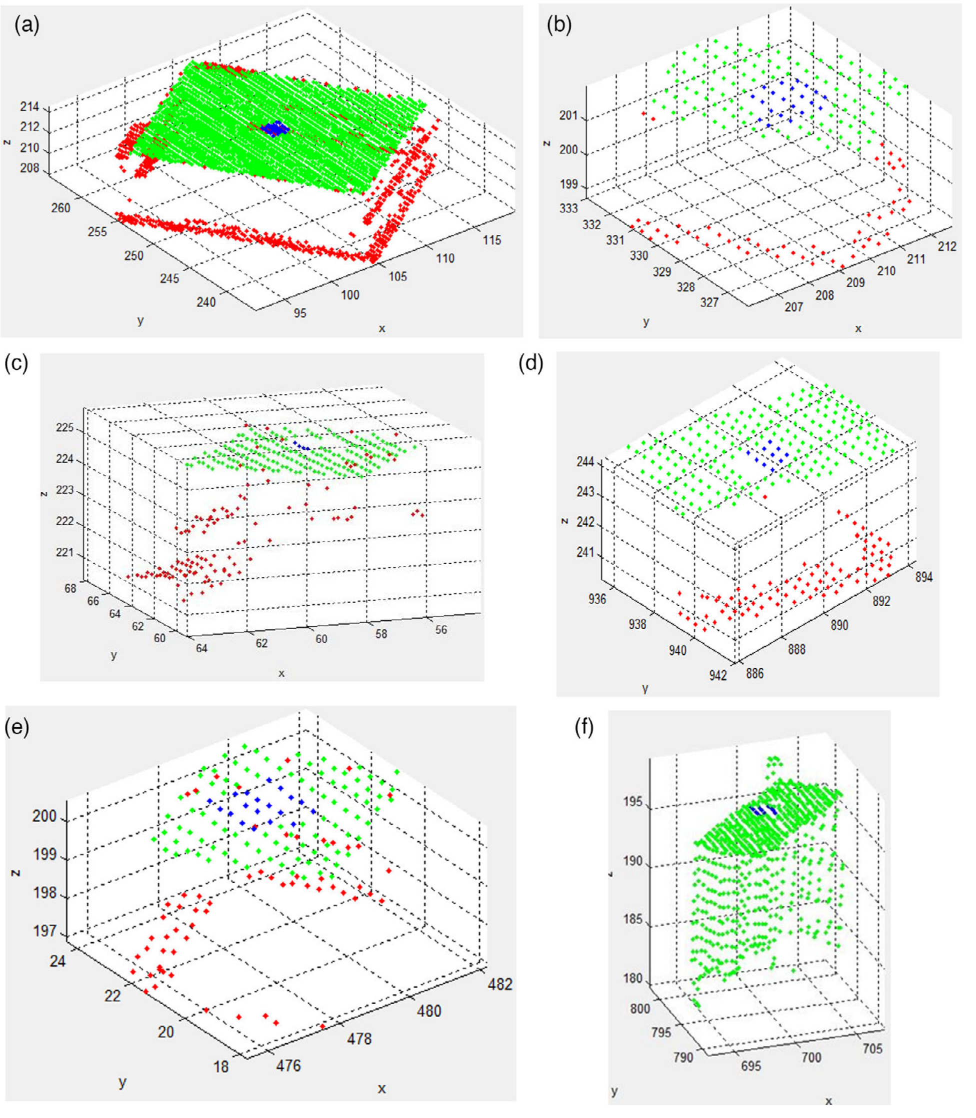


FIG. 4. Results using the proposed approach using LAD in the first step of the improved Li method. Blue points represent the extracted points for calculation by LAD; green points are the extracted points; red points represent the detected non-planar roof points.

### *Investigation of the Blunder Detection Ability of the Improved Li Method*

This subsection discusses the blunder detection ability of the improved Li method using the F201 dataset. This dataset consisted of both roof points and wall points; the vertical distance from the roof to the ground was about 14 m. The total number of lidar points was 678. The following lidar points used for the test were acquired using different vertical distances from the rooftop centroid as different thresholds. The results of the

TABLE V. Results of the proposed improved approach (including LAD) for the F16 and F201 datasets.

| | | | | |
|---|---|---|---|---|
| F16 | Centroid | E 215 058.457 m | Coordinate difference | E −0.468 m |
| | | N 2 647 063.404 m | | N 0.07 m |
| | | H 224.921 m | | H 0.053 m |
| | Fitting standard deviation | 0.02 m | No. of detected non-roof points | **107** |
| | Total points | 299 | Rate of detected non-roof points | **36%** |
| **F201** | Centroid | E 215 700.189 m | Coordinate difference | **E −0.141 m** |
| | | N 2 646 796.856 m | | **N −1.387 m** |
| | | H 192.335 m | | **H 3.742 m** |
| | Fitting standard deviation | 4.081 m | No. of detected non-roof points | **Undetected** |
| | Total points | 678 | Rate of detected non-roof points | **Unavailable** |

Problematic dataset shown in **bold**.

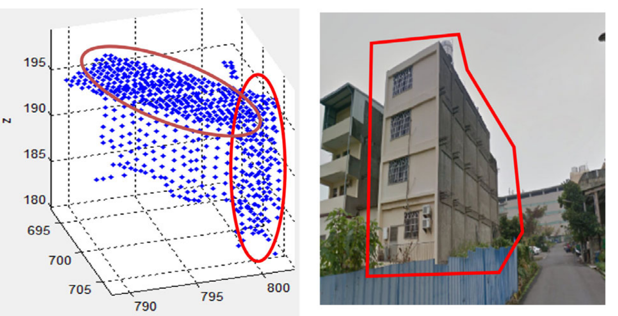


(a) (b)

FIG. 5. The lidar point distribution in the F201 dataset: (a) point cloud; (b) close-range image. The red ellipses in (a) indicate both the roof points and problematic wall points.

extracted roof points using the (original) Li method and the improved Li method were compared, and the evaluations were performed using the 3D coordinate differences between the centroids of the extracted points and the centroid determined from four roof corners surveyed by a total station. The results are shown in Table VI, in which the blue points indicate the points excluded by the vertical distance thresholds, the red points represent the detected non-planar roof points and the green points represent the extracted roof points.

From the first three vertical distance thresholds (1, 2 and 5 m), most of the wall points were excluded, and both the original Li and improved Li methods could extract the roof points correctly. The rate of the detected non-planar roof points was 9%, 15% and 29%, respectively, meaning that these two methods had the same ability to detect and locate non-planar roof points.

However, when 8 m was set as the vertical distance threshold for the test, the blunder detection ability of the original Li method was lost. As shown in Table VI, only 23% of the non-planar roof points could be located by the original Li method, however, 39% of the non-planar roof points could be located correctly using the improved Li method. Because of the poor detection of the original Li method, the coordinate differences in E, N, H were −0.157, 0.460 and 0.425 m, as shown in Table VI. For the other correct detections, the coordinate differences in E, N, H were −0.132, 0.163 and 0.059 m, no matter which method was used. However, when 8.5 m was set as the vertical distance threshold for the

TABLE VI. Comparison of results of different vertical distance thresholds (1 and 2 m in upper half; 5 and 8 m in lower half). In the point cloud images, blue points indicate the points excluded by the vertical distance thresholds, red points represent the detected non-planar roof points and green points represent the extracted roof points.

| *Threshold* | | *1 m* | | *2 m* | |
|---|---|---|---|---|---|
| *Method* | | *Improved Li method* | *Original Li method* | *Improved Li method* | *Original Li method* |
| Coordinate difference | E (m) | −0.132 | −0.132 | −0.132 | −0.132 |
| | N (m) | 0.163 | 0.163 | 0.163 | 0.163 |
| | H (m) | 0.059 | 0.059 | 0.059 | 0.059 |
| Total points | | 348 | | 371 | |
| No. of detected non-roof points | | 32 | 32 | 55 | 55 |
| Rate of detected non-roof points | | 9% | 9% | 15% | 15% |
| | | 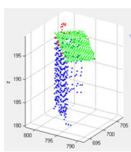 | 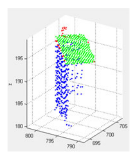 | 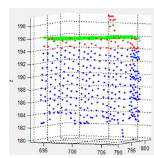 | 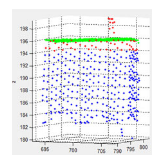 |
| *Threshold* | | *5 m* | | *8 m* | |
| *Method* | | *Improved Li method* | *Original Li method* | *Improved Li method* | *Original Li method* |
| Coordinate difference | E (m) | −0.132 | −0.132 | −0.132 | −0.157 |
| | N (m) | 0.163 | 0.163 | 0.163 | 0.460 |
| | H (m) | 0.059 | 0.059 | 0.059 | 0.425 |
| Total points | | 443 | | 522 | |
| No. of detected non-roof points | | 127 | 127 | 206 | **122** |
| Rate of detected non-roof points | | 29% | 29% | 39% | **23%** |
| | | 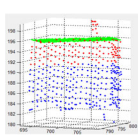 | 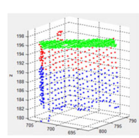 | 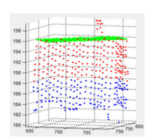 | 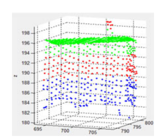 |

test, the blunder detection ability of the improved Li method was lost, as shown in Table VII. In this test, the proposed approach increased the detection rate by about 10%.

*Comparison with RANSAC.* Random sample consensus is a widely adopted method for the extraction of roof lidar points because of its robustness to noise and outliers. RANSAC can detect all points of the original cloud belonging to the calculated plane according to a given threshold. Afterwards, it repeats these procedures $N$ times and compares each obtained result with the previously saved one. If the new result is better, it replaces the saved result. In this study, the results of RANSAC for the F201 dataset are as shown in Table VIII using thresholds of 5 and 10 cm. Although the rates of non-planar roof points that could be detected by RANSAC is a little over 50% however the threshold

TABLE VII. Tabulated comparison results for the 8.5 m vertical distance threshold for the improved Li method.

| *Threshold* | | *8.5 m* | |
|---|---|---|---|
| Coordinate difference | E (m) | **−0.145** | 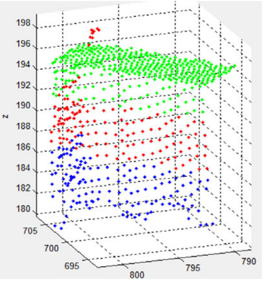 |
| | N (m) | **−0.432** | |
| | H (m) | **0.402** | |
| Total points | | 534 | |
| Number of detected non-roof points | | 137 | |
| Rate of detected non-roof points | | **26%** | |

TABLE VIII. Tabulated comparison results of different thresholds using RANSAC.

| *Threshold* | | *5 cm* | | *10 cm* | |
|---|---|---|---|---|---|
| Coordinate difference | E (m) | −0.064 | 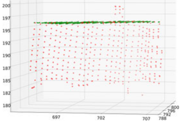 | −0.132 | 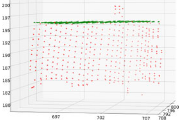 |
| | N (m) | 0.206 | | 0.162 | |
| | H (m) | 0.061 | | 0.061 | |
| Total points | | | | 678 | |
| No. of detected non-roof points | | 390 | | 362 | |
| Rate of detected non-roof points | | 58% | | 53% | |

should be set up. According to the results presented by Tarsha-Kurdi et al. (2008), in extreme situations RANSAC can provide unacceptable errors. These errors can be explained by the use of a purely mathematical principle, without considering the particularities of a building's lidar data cloud. McGlone et al. (2004) noted that the RANSAC algorithm aims to significantly reduce the number of necessary trials for large *N* values. However, it reduces *N* at the expense of having no guarantee of providing a solution free of gross errors, meaning there is no guarantee of obtaining the same result after each iteration. Although the proposed improved Li method did not perform as well as RANSAC, it can, nevertheless, obtain the same result. Additionally, only the rate of change of the a posteriori variance between the last and the previous iterations should be set (see equation (14)). Furthermore, the *K* value (1 or 3.29) should be set statistically to detect the blunders during iterations by considering the particularities of the building's lidar data cloud. However, the threshold of RANSAC, 5 or 10 cm, was set purely based on a rule of thumb, such as the expected planar accuracy.

### *Investigation Using ISPRS Vaihingen Dataset*

This subsection discusses roof point extraction using the ISPRS Vaihingen dataset in Germany, using the proposed improved Li method. The training file of the ISPRS Vaihingen data used for the investigation was Vaihingen3D_Traininig.pts, in which each point is labelled as powerline, low vegetation, impervious surfaces, car, fence/hedge, roof, façade, shrub or tree. The extraction using the proposed method was used to evaluate the classification results of the roof points and non-planar roof points according to a classification confusion matrix.

Because the proposed method extracted only points on one roof, a manual operation was performed to obtain the test data. Meanwhile, only label information was given in the test data, and the classification accuracy and precision were investigated instead of the geometric accuracy. Fig. 6 demonstrates the test data, including six pitched (sloping) roofs (the three gable-roofed buildings, indicated by the yellow rectangle) and seven horizonal roofs (indicated by the blue rectangle). The rate of non-planar roof points ranged from 9.4% to 53.7%, as shown in Tables IX and X. Tables IX and X also demonstrate the results of the roof point extraction of the ISPRS dataset using the proposed improved Li method. From Tables IX and X, roof no. 4-7 has a high rate of non-planar roof points (53.7%), leading to the wrong extraction. The other planar roof points were all extracted, meaning the successful classification of such roof points.

In particular, roof no. 4-6 contained 51.7% non-planar roof points, however, the proposed method could still extract the planar roof points successfully. It showed more impressive results than those in the simulated and Taiwan data. Additionally, the classification accuracy and precision were 84.4% and 81.6% for roof no. 4-2 and 77.4% and 69.3% for roof no. 4-6. The classification accuracy and precision for the other roofs were all higher than 90%. Importantly, the recall for all successful extractions were higher than 90%.

For the 12 successfully extracted roof planes, the omission error (1-recall) was less than 7%. Among them, roof nos. 4-2 and 4-6 had a higher commission error (1-precision; false positive; type I error) and the plane fitting might be affected. The commission error for the other four horizontal roofs was less than 6%, and the commission error of the six sloping roofs was 0%. Meanwhile, the detected roof points contained more than 600 points, which meant that the plane fitting was not affected.

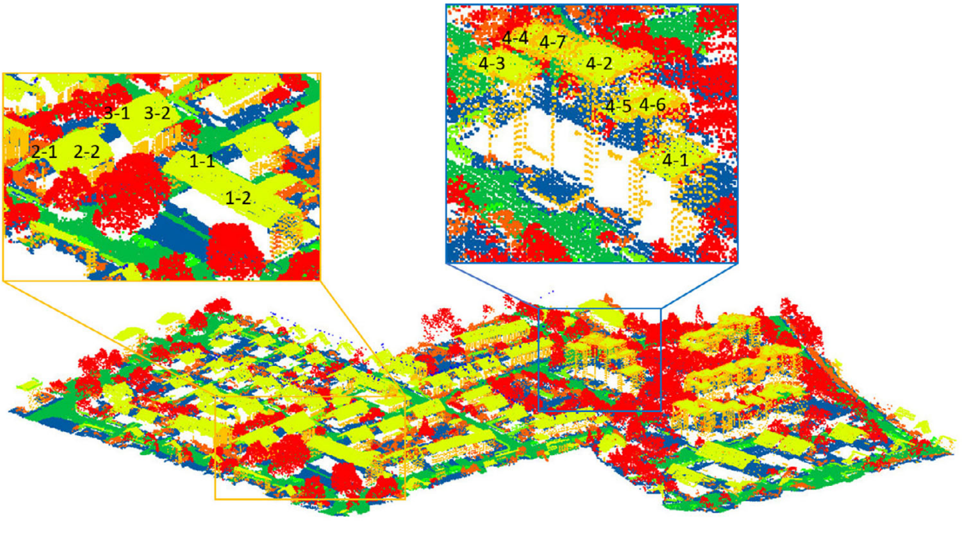


Fig. 6. Distribution of the test lidar points in the ISPRS Vaihingen dataset. Roof points are shown in light green. Other colours represent non-planar roof points, including powerlines, low vegetation, impervious surfaces, cars, fence/hedges, façades, shrubs and trees.

TABLE IX. Gable (sloping) roof point extraction from the ISPRS Vaihingen dataset using the improved Li method (on righ-hand images, blue: roof points; orange: omission points; red: non-roof points; green: commission points).

| *Roof No.1-1* | *Roof pts.* | *Non-roof pts.* | *SUM* | *Precision* |
|---|---|---|---|---|
| Extracted roof pts. | 2906 | 0 | 2906 | 100·0% |
| Extracted non-roof pts. | 161 | 839 | 1000 | The rate of non-roof pts. |
| SUM | 3067 | 839 | 3906 | |
| Recall | 94·8% | Accuracy | 95·9% | 21·5% |

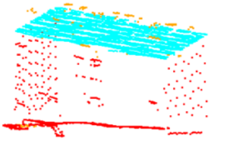

| *Roof No.1-2* | *Roof pts.* | *Non-roof pts.* | *SUM* | *Precision* |
|---|---|---|---|---|
| Extracted roof pts. | 2928 | 0 | 2928 | 100·0% |
| Extracted non-roof pts. | 66 | 309 | 375 | The rate of non-roof pts. |
| SUM | 2994 | 309 | 3303 | |
| Recall | 97·8% | Accuracy | 98·0% | 9·4% |

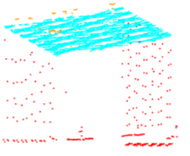

| *Roof No.2-1* | *Roof pts.* | *Non-roof pts.* | *SUM* | *Precision* |
|---|---|---|---|---|
| Extracted roof pts. | 1658 | 0 | 1658 | 100·0% |
| Extracted non-roof pts. | 111 | 192 | 303 | The rate of non-roof pts. |
| SUM | 1769 | 192 | 1961 | |
| Recall | 93·7% | Accuracy | 94·3% | 9·8% |

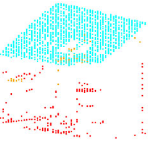

| *Roof No.2-2* | *Roof pts.* | *Non-roof pts.* | *SUM* | *Precision* |
|---|---|---|---|---|
| Extracted roof pts. | 2258 | 0 | 2258 | 100·0% |
| Extracted non-roof pts. | 45 | 539 | 584 | The rate of non-roof pts. |
| SUM | 2303 | 539 | 2842 | |
| Recall | 98·0% | Accuracy | 98·4% | 19·0% |

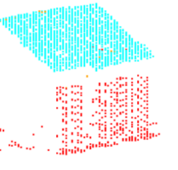

| *Roof No.3-1* | *Roof pts.* | *Non-roof pts.* | *SUM* | *Precision* |
|---|---|---|---|---|
| Extracted roof pts. | 1542 | 0 | 1542 | 100·0% |
| Extracted non-roof pts. | 11 | 593 | 604 | The rate of non-roof pts. |
| SUM | 1553 | 593 | 2146 | |
| Recall | 99·3% | Accuracy | 99·5% | 27·6% |

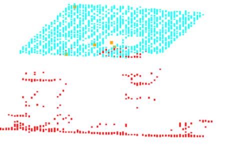

| *Roof No.3-2* | *Roof pts.* | *Non-roof pts.* | *SUM* | *Precision* |
|---|---|---|---|---|
| Extracted roof pts. | 2001 | 0 | 2001 | 100·0% |
| Extracted non-roof pts. | 73 | 880 | 953 | The rate of non-roof pts. |
| SUM | 2074 | 880 | 2954 | |
| Recall | 96·5% | Accuracy | 97·5% | 29·8% |

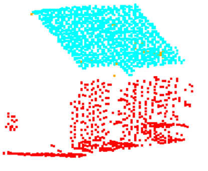

TABLE X. Horizontal roof point extraction from ISPRS Vaihingen dataset using improved Li method. (on right-hand images, blue: roof points; orange: omission points; red: non-roof points; green: commission points).

| | | | | | |
|---|---|---|---|---|---|
| *Roof No.4-1* | *Roof pts.* | *Non-roof pts.* | *SUM* | *Precision* | 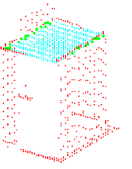 |
| Extracted roof pts. | 794 | 34 | 828 | 95·9% | |
| Extracted non-roof pts. | 1 | 506 | 507 | The rate of non-roof pts. | |
| SUM | 795 | 540 | 1335 | | |
| Recall | 99·9% | Accuracy | 97·4% | 40·5% | |
| *Roof No.4-2* | *Roof pts.* | *Non-roof pts.* | *SUM* | *Precision* | 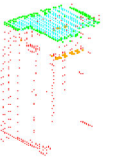 |
| Extracted roof pts. | 913 | 206 | 1119 | **81·6%** | |
| Extracted non-roof pts. | 34 | 390 | 424 | The rate of non-roof pts. | |
| SUM | 947 | 596 | 1543 | | |
| Recall | 96·4% | Accuracy | **84·5%** | 38·6% | |
| *Roof No.4-3* | *Roof pts.* | *Non-roof pts.* | *SUM* | *Precision* |  |
| Extracted roof pts. | 637 | 40 | 677 | 94·1% | |
| Extracted non-roof pts. | 2 | 535 | 537 | The rate of non-roof pts. | |
| SUM | 639 | 575 | 1214 | | |
| Recall | 99·7% | Accuracy | 96·5% | 47·4% | |
| *Roof No.4-4* | *Roof pts.* | *Non-roof pts.* | *SUM* | *Precision* | 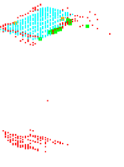 |
| Extracted roof pts. | 765 | 30 | 795 | 96·2% | |
| Extracted non-roof pts. | 2 | 263 | 265 | The rate of non-roof pts. | |
| SUM | 767 | 293 | 1060 | | |
| Recall | 99·7% | Accuracy | 97·0% | 27·6% | |
| *Roof No.4-5* | *Roof pts.* | *Non-roof pts.* | *SUM* | *Precision* | 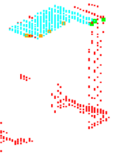 |
| Extracted roof pts. | 600 | 3 | 603 | 99·5% | |
| Extracted non-roof pts. | 5 | 377 | 382 | The rate of non-roof pts. | |
| SUM | 605 | 380 | 985 | | |
| Recall | 99·2% | Accuracy | 99·2% | 38·6% | |
| *Roof No.4-6* | *Roof pts.* | *Non-roof pts.* | *SUM* | *Precision* | 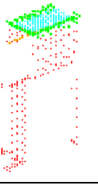 |
| Extracted roof pts. | 339 | 150 | 489 | **69·3%** | |
| Extracted non-roof pts. | **16** | 230 | 246 | The rate of non-roof pts. | |
| SUM | 355 | 380 | 735 | | |
| Recall | 95·5% | Accuracy | **77·4%** | 51·7% | |
| *Roof No.4-7* | *Roof pts.* | *Non-roof pts.* | *SUM* | *Precision* | 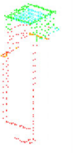 |
| *Extracted roof pts.* | *281* | *197* | *478* | *58·8%* | |
| *Extracted non-roof pts.* | *25* | *158* | *183* | *The rate of non-roof pts.* | |
| *SUM* | *306* | *355* | *661* | | |
| *Recall* | *91·8%* | *Accuracy* | *66·4%* | *53·7%* | |

Fig. 7 shows the combined results of the planar roof point extraction, in which incorrect extractions are indicated by a black circle. The same test data was also used to extract the planar roof points by the original Li method. Table XI shows the differences using the original and improved Li methods. Roof no. 4-7 could not be extracted successfully by the original Li method because of the high rate of non-planar roof points. The roof points of roof nos. 3-2 and 4-6 also could not be extracted successfully. The reasons for the unsuccessful extractions were because a better initial value could not be obtained for roof no. 3-2 and the high rate of non-planar roof points, 51.7%, for roof no. 4-6. This result proved again that the improved Li method could obtain a better initial value from LAD and could deal with more blunders than the original Li method. Table XI illustrates the extraction results of roof nos. 3-2 and 4-6 using the original and improved Li methods.

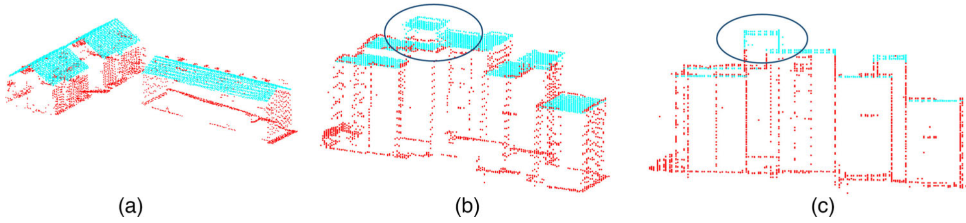


Fig. 7. Combined results of the planar roof point extraction using selected test data in the ISPRS Vaihingen dataset: (a) six roofs of three gabled buildings; (b) seven horizontal roofs; (c) side view of the seven horizontal roofed buildings. Blue: correct roof points. Red: non-roof points. Incorrect roof extractions are indicated by the black circles.

Table XI. Differences of the planar roof point extraction from the ISPRS Vaihingen dataset using the original Li method and the improved Li method.

| | | |
|---|---|---|
| *Roof no. 3-2* Rate of non-roof points: 29.8% | 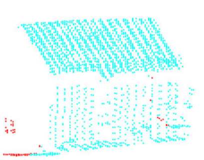 (a) Original Li method | 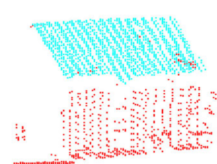 (b) Improved Li method |
| *Roof no. 4-6* Rate of non-roof points: 51.7% | 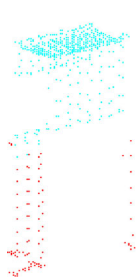 (c) Original Li method | 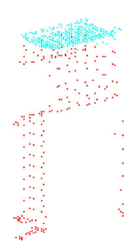 (d) Improved Li method |

Blue, roof points; Red, non-roof points.

Therefore, the test results of actual Taiwan and ISPRS Vaihingen datasets proved that the proposed approach was more robust than the original Li method. It also demonstrated the applicability, as well as the effectiveness, of the proposed method in extracting lidar planar roof points.

## Conclusions

This study has developed a least-squares fitting approach based on iterations supervised by a posteriori variance estimation (Li, 1983; Li et al., 2015), called the Li method, to reduce the weights of non-planar roof points during the iterative process in order to extract planar roof points more accurately. Additionally, least absolute deviation (LAD) was integrated into the first step of the original Li method and the resulting improved Li method increases the blunder detection ability.

Both simulated and actual airborne lidar datasets were used to verify the developed algorithm. The results showed that the proposed method was robust and resistant to blunders. It proved that a better parameter estimation is important for the Li method in the initial step and the LAD method can acquire better planar parameter estimations for the Li method. It also proved that the improved Li method, combined with LAD as the first step of the Li method, can increase the detection rate of blunders. This is because LAD can determine better planar parameter estimations in the first step than in the original Li method. However, a large number of blunders can still lead to the failure of the improved Li method.

The simulated test results showed that the detected and located percentage of blunders were about 35% and 40% when the blunder sizes were 0.4 and 0.5 m, respectively. The detected and located percentages of blunders were both 44% when the blunder sizes were 1 and 2 m. The proposed approach improved the detection rate of small blunders of 0.4 and 0.5 m by about 2% and 5%, respectively, and improved the detection rate of larger blunders (1 or 2 m) by about 6%, compared to the original Li method. Additionally, after the actual Taiwan data test, 39% of the non-planar roof points could be located correctly by the proposed approach, showing an improvement to the detection rate of about 10%. When using the ISPRS Vaihingen dataset, only one roof (containing 53.7% non-planar roof points) failed to be extracted; the proposed method extracted roof points on 12 roofs successfully, even including one roof containing 51.7% non-planar roof points. It showed more impressive results than those in the simulated and Taiwan data. Moreover, the classification accuracy and precision for 10 of the roofs were all higher than 90%. Importantly, the recall for all 12 successful extractions reached 90%. Therefore, the test results of the actual Taiwan and ISPRS Vaihingen datasets demonstrated that the proposed approach was more robust than the original Li method. It also proved the applicability, as well as effectiveness, of the proposed method in extracting lidar planar roof points.

## Acknowledgements

The authors would like to record their appreciation to the National Land Surveying and Mapping Center, Taiwan (ROC), who provided the Taiwan test data.

## References

Ackermann, F., 1999. Airborne laser scanning – present status and future expectations. *ISPRS Journal of Photogrammetry and Remote Sensing*, 54(2–3): 64–67.

Axelsson, P., 2000. DEM generation from laser scanner data using adaptive TIN models. *International Archives of Photogrammetry and Remote Sensing*, 33(B4/1): 110–117.

Baarda, W., 1967. A testing procedure for use in geodetic networks. *Publications on Geodesy 9*, 2(5). Netherlands Geodetic Commission, Delft, The Netherlands. 97 pages.

Ballard, D. H. and Brown, C. M., 1982. *Computer Vision*. Prentice-Hall, Englewood Cliffs, New Jersey, USA. 523 pages.

Boscovich, R. J., 1757. De literraria expeditione per pontificiam synopsis amplioris operis, ac habentur plura eius ex exempla ria etiam sensorum impressa. *Commentarii de Bononiensi Scientiarum et Artium Instituto Atque Academia*, 4: 353–396.

Chan, L. C. and Chio, S.-H., 2017. Least squares planar roof fitting from airborne lidar point cloud using iteration with the selected weights. *International Symposium on Remote Sensing (ISRS 2017)*, Nagoya, Japan. 4 pages (on CD-ROM).

Chio, S.-H., 2005. Automatic extraction of 3-D building roofs by data snooping from airborne LIDAR data. *26th Asian Conference on Remote Sensing (ACRS2005)*, Hanoi, Vietnam. 1: 1841–1849.

Chio, S.-H., 2008. A study on roof point extraction based on robust estimation from airborne LiDAR data. *Journal of the Chinese Institute of Engineers*, 31(4): 537–550.

Dantzig, G. B., 1987. Origins of the simplex method. *Technical Report SOL 87-5*, Systems Optimization Laboratory, Department of Operations Research, Stanford University, Stanford, California, USA. 13 pages.

Dey, E. K., Awrangjeb, M. and Stantic, B., 2020. Outlier detection and robust plane fitting for building roof extraction from LiDAR data. *International Journal of Remote Sensing*, 41(16): 6325–6354.

Fischler, M. A. and Bolles, R. C., 1981. Random sample consensus: a paradigm for model fitting with application to image analysis and automated cartography. *Communications of the ACM*, 24(6): 381–395.

Forlani, G., Nardinocchi, C., Scaioni, M. and Zingaretti, P., 2003. Building reconstruction and visualization from LIDAR data. *International Archives of Photogrammetry, Remote Sensing and Spatial Information Sciences*, 34(5/W12): 151–156.

Geibel, R. and Stilla, U., 2000. Segmentation of laser altimeter data for building reconstruction: different procedures and comparison. *International Archives of Photogrammetry and Remote Sensing*, 33(B3): 326–334.

Gorte, B., 2002. Segmentation of TIN-structured surface models. *Joint International Symposium on Geospatial Theory, Processing and Applications*, Ottawa, Canada. 5 pages (on CD-ROM).

Haala, N. and Brenner, C., 1999. Extraction of building and trees in urban environments. *ISPRS Journal of Photogrammetry and Remote Sensing*, 54(2–3): 130–137.

Höhle, J., 2013. Assessing the positional accuracy of airborne laser scanning in urban areas. *Photogrammetric Record*, 28(142): 196–210.

Khoshelham, K., 2005. Region refinement and parametric reconstruction of building roofs by integration of image and height data. *International Archives of Photogrammetry, Remote Sensing and Spatial Information Sciences*, 36(3/W24): 3–8.

Li, D., 1983. Ein Verfahren zur Aufdeckung großer Fehler mit Hilfe der a-posteriori Varianzschätzung. *Bildmessung und Luftbildwesen*, 51(5): 184–187.

Li, D., Wang, S. and Li, D., 2015. *Spatial Data Mining: Theory and Application*. Springer-Verlag, Berlin, Germany. 308 pages.

Maas, H.-G. and Vosselman, G., 1999. Two algorithms for extracting building models from raw laser altimetry data. *ISPRS Journal of Photogrammetry and Remote Sensing*, 54(2–3): 153–163.

McGlone, J. C., Mikhail, E. M. and Bethel, J. S. (Eds.), 2004. *Manual of Photogrammetry*. Fifth edition. ASPRS, Bethesda, Maryland, USA. 1151 pages.

Mikhail, E. M. and Ackermann, F. E., 1976. *Observation and Least Squares*. IEP, New York, USA. 497 pages.

Priestnall, G., Jaafar, J. and Duncan, A., 2000. Extracting urban feature from LiDAR digital surface models. *Computers, Environment and Urban Systems*, 24(2): 65–78.

Roggero, M., 2002. Object segmentation with region growing and principal component analysis. *International Archives of Photogrammetry, Remote Sensing and Spatial Information Sciences*, 34(3A): 289–294.

Schuster, H. F., 2004. Segmentation of LIDAR data using the tensor voting framework. *International Archives of Photogrammetry, Remote Sensing and Spatial Information Sciences*, 35(B3): 1073–1078.

Sisman, Y., 2010. Outlier measurement analysis with the robust estimation. *Scientific Research and Essays*, 5(7): 668–678.

Tarsha-Kurdi, F., Landes, T. and Grussenmeyer, P., 2008. Extended RANSAC algorithm for automatic detection of building roof planes from Lidar data. *Photogrammetric Journal of Finland*, 21(1): 97–109.

Vosselman, G. and Dijkman, S., 2001. 3D Building model reconstruction from point clouds and ground plans. *International Archives of Photogrammetry and Remote Sensing*, 34(3/W4): 37–43.

Wang, M. and Tseng, Y.-H., 2004. LIDAR data segmentation and classification based on octree structure. *International Archives of Photogrammetry, Remote Sensing and Spatial Information Sciences*, 35(B3): 308–313.

Williams, G., 2017. *Linear Algebra with Applications*. Ninth edition. Jones and Bartlett, Burlington, Massachusetts, USA. 594 pages.

## *Résumé*

*La méthode d'ajustement par moindres carrés peut être utilisée pour l'extraction de points de toits plans à partir de points d'un levé lidar aéroporté; cependant, elle ne peut pas éviter l'impact des points de toits non plans (aberrations) dus à un manque de robustesse. Cette étude a donc développé une méthode d'ajustement de plan par moindres carrés basée sur l'estimation a posteriori de la variance, telle que proposée par Li en 1983, pour réduire le poids des points de toit non plans. De plus, la moindre déviation absolue a été intégrée à la première étape de cette méthode Li améliorée, pour accroître la détection des aberrations. Pour les données simulées, l'approche proposée a augmenté le taux de détection des aberrations jusqu'à 6% par rapport à la méthode Li originale. Les résultats des tests sur des données réelles ont démontré la robustesse, l'applicabilité et l'efficacité de l'approche proposée.*

## *Zusammenfassung*

*Die Kleinste-Quadrate-Methode kann für die Extraktion ebener Dachflächenpunkte aus Lidar-Punktwolken genutzt werden. Dennoch kann damit der Einfluss von nicht-ebenen Dachpunkten (Ausreißern) durch fehlende Robustheit nicht abgefangen werden. Diese Studie stellt eine Ebeneneinpassung mittels Kleinster-Quadrate Methode vor, die sich auf eine posteriori Varianzschätzung stützt, wie bereits von Li im Jahr 1983 vorgeschlagen, um die nicht-ebenen Dachpunkte herunter zu gewichten. In diese verbesserte Methode nach Li wurde zusätzlich der Ansatz der kleinsten absoluten Abweichung (LAD) in den ersten Schritt integriert, um die Erkennungsrate von Ausreißern zu erhöhen. Für simulierte Daten steigert der vorgeschlagene Ansatz die Erkennungsrate von Ausreißern um 6% verglichen mit der originalen Li-Methode. Empirische Tests mit realen Daten zeigen die Robustheit, Anwendbarkeit und Effektivität der vorgeschlagenen Methode.*

## *Resumen*

*El método de ajuste de mínimos cuadrados se puede utilizar para la extracción de puntos en cubiertas planas a partir de puntos de LIDAR aeroportado; sin embargo, debido a la falta de robustez no puede evitar el impacto de puntos del tejado que no están en el plano (errores). Por tanto, en este estudio ha desarrollado un método de ajuste de planos por mínimos cuadrados basado en una estimación de la varianza a posteriori, como propuso Li en 1983, reduciendo el peso de los puntos de cubierta que no están en el plano. Además, la desviación mínima absoluta (LAD) se integró en el primer paso de este método mejorado de Li, para aumentar la detección de errores. Con datos simulados, el enfoque propuesto aumentó la tasa de detección de errores hasta en un 6% en comparación con el método de Li original. Los resultados con datos reales mostraron la robustez, aplicabilidad y eficacia del método propuesto.*

## 摘要

最小二乘拟合方法可用于机载激光雷达点的平面屋顶点提取；然而，由于缺乏鲁棒性，它无法避免非平面屋顶点（错误）的影响。因此，本研究开发了一种基于后验方差估计的最小二乘平面拟合方法，由李在 *1983* 年提出，以减少非平面屋顶点的权重。此外，最小绝对偏差 *(LAD)* 被整合到这种改进的锂方法的第一步中，以增加错误检测。对于模拟数据，与原始 *Li* 方法相比，所提出的方法将错误检测率提高了 *6%*。真实数据的测试结果表明，所提出的方法具有稳健性、适用性和有效性。